Dalton Transactions

ROYAL SOCIETY OF CHEMISTRY

PAPER

View Article Online
View Journal | View Issue

Check for updates

Cite this: *Dalton Trans.*, 2025, **54**, 5796

Charge transfer between a metal-bound halide and a quinone through π-hole interactions leads to bulk conductivity†

Lidija Molčanov, [a] Anna Krawczuk, *[b] Luka Pavić,[a] Marijana Jurić, [a] Lidija Androš Dubraja [a] and Krešimir Molčanov *[a]

Received 23rd October 2024,
Accepted 19th February 2025

DOI: 10.1039/d4dt02961e

rsc.li/dalton

π-Hole interactions between a metal-bound halide and a quinoid ring are described in four novel isostructural co-crystals with the formula [Cu(terpy)ClX]·X′$_4$Q (terpy = 2,2′:6′,2″-terpyridine; Q = quinone; X = Br, I; X′ = Cl, Br). An unusually strong π-hole interaction between Cu–X and the quinoid ring is noted. Periodic DFT computations estimate the energy of the X···quinone interaction to be −20.79 kcal mol^{-1}, indicating a very strong non-covalent interaction attributed to a higher degree of polarization along the bonding path. The black colour of the crystals originates from a cooperative intermolecular charge transfer between the [Cu(terpy)ClX] complex and the quinone π-system, with iodine playing a dominant role in this process by facilitating the π-hole interaction that enhances the charge transfer mechanism. All the compounds are considered to be weak semiconductors with the σ_{DC} magnitude ranging between 10^{-11} and 10^{-9} S cm^{-1}. It is anticipated that by a smart choice of electron donors and electron acceptors, one can substantially enhance the effect and engineer more efficient conductive materials.

Introduction

Metal–organic systems combining a transition metal complex and an uncoordinated organic electron donor/acceptor are a promising area for the design of novel multifunctional molecular materials.[1–4] Transition metal atoms with their unpaired electrons allow tuning of magnetic properties, while organic donors/acceptors allow the transfer of charge. Most commonly, conductivity is achieved through π-stacking of organic radicals,[1,5–13] but other mechanisms of conductivity are being studied, such as stacking between organic guest molecules and organic ligands bound to a metal.[14] However, this type of contact rarely involves charge transfer.[15–17] A less-studied mechanism is through anion–π interactions,[18,19] which may also involve charge transfer.[20,21] These involve areas of electron depletion in π-electron systems (π-holes) which often form attractive interactions with electron-rich or electron-donating groups.[22–36] The interactions are mostly of electrostatic nature and form when an electron-rich moiety is in close contact with an area of depleted electron density. One of the mechanisms responsible for the effect involves charge transfer from a donor lone pair to an antibonding orbital of the acceptor π system (n → π* charge transfer).[23,26,28,30] The colour of the compound is a good indicator of charge transfer: charge-transfer systems are typically intensely coloured and usually considerably darker than constituent compounds. Colour intensity and opacity can thus serve as a rough estimate of the degree of charge transfer.

For example, co-crystals of perhalogenoquinones (which have especially prominent π-holes) with halide anions are black due to strong n → π* charge transfer.[37–39] Electron depletion of the quinoid ring facilitates electron transfer from a halide lone pair to a π* orbital of quinone. The nature of quinone–iodide interactions[40] was recently studied on a model co-crystal of 3-chloro-*N*-methylpyridinium iodide and tetrabromoquinone (Br$_4$Q) and was confirmed to be n → π* with approximately 10% of charge transferred from the iodide anion to the quinone, and the attractive interaction has been estimated to be −11 kcal mol^{-1},[41] surpassing most weak non-covalent interactions, including hydrogen bonds. Since the formation of these quinone–halogen interactions is energetically very favourable, their appearance in crystals is highly predictable and a sandwich-like 'supramolecular synthon' iodide···quinone···iodide has been observed in quite a number of compounds.[37,39] Thus, π-hole interactions have become interesting not only in crystal engineering,[21,24,25,27,29,30,36] but also in molecular recognition[25,31,42] and drug design.[26]

It would be interesting to use this type of interaction in the design of novel metal–organic systems. However, contacts of

[a]*Rudjer Bošković Institute, Bijenička 54, HR-10000 Zagreb, Croatia. E-mail: kmolcano@irb.hr*
[b]*Institut für Anorganische Chemie, University of Göttingen, Tammanstraße 4, D-37077 Göttingen, Germany. E-mail: anna.krawczuk@uni-goettingen.de*

†Electronic supplementary information (ESI) available. CCDC 2310494–2310497. For ESI and crystallographic data in CIF or other electronic format see DOI: https://doi.org/10.1039/d4dt02961e

metal-bound halides with quinones and other similar electron acceptors (such as 7,7,8,8-tetracyanoquinodimethane, triazine, tetracyanoethylene, *etc.*), although not unknown,[43] are not very common. In most cases, the distances between the halide and ring centroid (or the ring mean plane) are too long to allow a meaningful charge transfer. Only a handful of close contacts with favourable geometry are found in the Cambridge Structural Database (CSD):[44] four with Cl,[45–47] four with Br[48] and one with I.[49]

In this work, we present a novel series of compounds with π-hole interactions between a metal-bound halide and a quinoid ring, involving inter- and intramolecular charge transfer. This unique motif is observed in four novel isostructural co-crystals with the formula [Cu(terpy)ClX]·X′4Q [terpy = 2,2′:6′,2″-terpyridine; Q = 1,4-benzoquinone; X = I, X′ = Cl (**1**); X = I, X′ = Br (**2**); X = Br, X′ = Cl (**3**); and X = Br, X′ = Br (**4**); Scheme 1].

Results and discussion

Coordination of the Cu(II) centre in compounds **1–4** is a distorted square pyramid with terpyridine and chloride ligands forming the basal plane and the halide X located at the apical position (Fig. S1–S4†). These complexes are similar to previously described [Cu(terpy)X_2] ($X = Br^-, I^-$) compounds where both halogens are the same element.[50,51] Nonetheless, the most interesting feature of the co-crystals is the presence of π-hole interactions where the halide anion interacts with a quinoid ring, being at the same time bonded to a metal centre. For a description of this interaction, we used previously proposed geometric parameters[37,39,41] shown in Fig. 1a: distance from the halide to the ring centroid, $d(C_g)$, distance from the halide to the ring mean plane, d(plane), angle between the halide···centroid axis and ring mean plane, α, and direction of offset defined as the inclination from the central O═C···C═O axis towards the substituent with the highest priority according to IUPAC rules,[52] β. However, due to the presence of a metal, we propose a new parameter, an angle γ between the Cu–X bond and the centroid of the quinoid ring (Fig. 1a, Table 1).

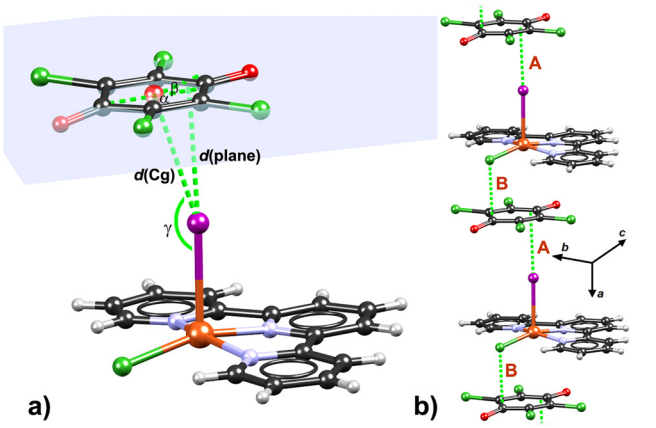

Fig. 1 (a) Short halogen-quinone π-hole contact in **1** with relevant geometric parameters (listed in Table 1) marked. $d(C_g)$ is the distance between a halide and the ring centroid, d(plane) is the distance between a halide and the ring mean plane, α is an angle between the halide···centroid axis and the ring mean plane, β is the direction of the offset and γ is the angle between the Cu–X bond and the ring centroid. Offset is calculated as $d(C_g)\cdot\cos(\alpha)$; (b) an infinite chain of π-hole interactions parallel to the *a*-axis. π-Hole contacts **A** and **B** are marked with red letters.

The π-hole interactions are studied by comparing the four analogous crystal structures of compounds **1–4**, and by quantum chemical modelling of the prototype compound, [Cu(terpy)ClI]·Cl_4Q (**1**).

There are two symmetry-independent π-hole interactions: the stronger one is formed by the halide X in the apical position (labelled as contact **A**, Fig. 1b), with a γ angle of about 160° (Fig. 1a). Distances between X and the quinone (Table 1) are somewhat shorter than in previously reported co-crystals of uncoordinated iodide,[37,39,41] indicating stronger interaction.

The weaker motif is formed by the Cl atom in an equatorial position (labelled as contact **B**, Fig. 1b) with a γ angle of 75–85°. This contact is part of a larger stacking interaction between the terpy ligand and the quinoid ring. Due to large offsets (>2 Å) and centroid distances exceeding 4.0 Å (Table S4†), the stacking interaction can be considered to be weak and of secondary importance.

Topological analysis of theoretically obtained electron density[53,54] for **1** (Tables 2 and S5†) revealed that the Cu–I bond is weaker than the other four coordination bonds. This is well-reflected by kinetic $G(\mathbf{r}_{CP})$ and potential $V(\mathbf{r}_{BCP})$ energy densities[55] estimated using the approximation given by Abramov:[56]

$$G(\mathbf{r}_{CP}) = \frac{3}{10}\left(3\pi^2\right)^{\frac{2}{3}}\rho^{\frac{5}{3}}(\mathbf{r}_{CP}) + \frac{1}{6}\nabla^2\rho(\mathbf{r}_{CP})$$

$$V(\mathbf{r}_{CP}) = \frac{\hbar^2}{4m}\nabla^2\rho(\mathbf{r}_{CP}) - 2G(\mathbf{r}_{CP})$$

It holds well in regions where $\nabla^2\rho(\mathbf{r}_{CP})$ is positive and is a good approximation for the transition metal–ligand bonds.[57] Both kinetic and potential energy densities are significantly

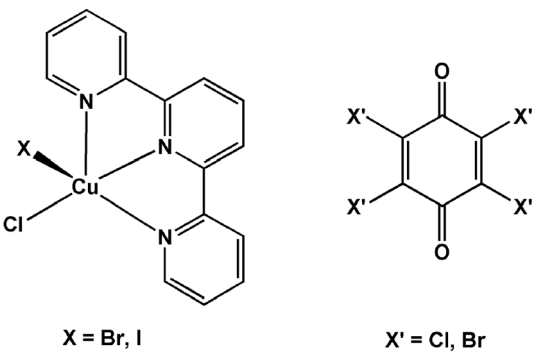

Scheme 1 The complex [Cu(terpy)ClX] (left) and tetrahalogenquinone (right).

Table 1 Geometric parameters of iodide···quinone interactions as defined in our previous work[37] and shown in Fig. 1. Symmetry operators: (i) −1/2 + *x*, 3/2 − *y*, 1/2 + *z*; (ii) 1/2 + *x*, 3/2 − *y*, 1/2 + *z*

	$d(C_g)$/Å	d(plane)/Å	α/°	β/°	γ/°	Offset/Å
1						
Cu1–I1···C1^{i} → C6^{i}	3.5836(19)	3.465	75.4	8.8	161.8	0.903
Cu1–Cl5···C1^{ii} → C6^{ii}	3.451(2)	3.160	66.3	3.3	76.9	1.387
2						
Cu1–I1···C1^{i} → C6^{i}	3.779(4)	3.598	74.3	15.5	161.5	1.029
Cu1–Cl1···C1^{ii} → C6^{ii}	3.592(4)	3.311	67.0	6.2	78.4	1.403
3						
Cu1–Br1···C1^{i} → C6^{i}	3.525(2)	3.419	77.4	23.2	163.8	0.769
Cu1–Cl5···C1^{ii} → C6^{ii}	3.44(4)	3.180	67.8	6.4	82.0	1.300
4						
Cu1–Br5···C1^{i} → C6^{i}	3.679(2)	3.459	71.6	22.7	160.0	1.161
Cu1–Cl1···C1^{ii} → C6^{ii}	3.543(3)	3.262	67.9	8.3	80.9	1.333

Table 2 Topological analysis of selected non-covalent interactions [(3,−1) critical points] between the [Cu(terpy)I$_2$] moiety and the tetrachloroquinone scaffold in **1**. The first row refers to calculations within boundary conditions and the second row with values given in *italics* refers to gas-phase calculations

	ρ(r)	$\nabla^2\rho$(r)	$G(\mathbf{r}_{CP})$	$V(\mathbf{r}_{CP})$	$E(\mathbf{r}_{CP})$	$\lvert V(\mathbf{r}_{CP})\rvert/G(\mathbf{r}_{CP})$	BP
I1···C1^{i}	0.050	0.694	0.03	−0.02	0.01	0.57	3.56
	0.119	*1.005*	*0.07*	*−0.07*	*0.00*	*0.96*	*3.53*
Cl5···C4^{ii}	0.057	0.906	0.05	−0.03	0.02	0.65	3.26
	0.066	*0.718*	*0.04*	*−0.04*	*0.01*	*0.83*	*3.22*
N1···Cl1^{ii}	0.029	0.559	0.03	−0.02	0.01	0.65	3.55
	0.038	*0.521*	*0.03*	*−0.02*	*0.01*	*0.78*	*3.57*
N2···O1^{ii}	0.031	0.442	0.03	−0.02	0.01	0.79	3.21
	0.034	*0.499*	*0.03*	*−0.02*	*0.01*	*0.72*	*3.27*
N3···Cl4^{ii}	0.033	0.621	0.03	−0.02	0.01	0.65	3.62
	0.042	*0.547*	*0.03*	*−0.03*	*0.01*	*0.79*	*3.59*

ρ(**r**) is given in e Å^{-3}, $\nabla^2\rho$(**r**), $G(\mathbf{r}_{CP})$ $V(\mathbf{r}_{CP})$ and electronic local energy density $E(\mathbf{r}_{CP})$ are given in e Å^{-5}, BP – bond path length in Å; symmetry codes: (i) −1/2 + *x*, 3/2 − *y*, 1/2 + *z*, (ii) 1/2 + *x*, 3/2 − *y*, 1/2 + *z*.

smaller (0.15 e Å^{-5} and −0.22 e Å^{-5}, respectively) than for other coordination bonds indicating its unique character. Interestingly, the ratio $\lvert V(\mathbf{r}_{CP})\rvert/G(\mathbf{r}_{CP})$ being 1.44 and Laplacian being only slightly positive (1.20 e Å^{-5}), both indicate that the Cu–I bond is the weakest coordination bond. Hence, for the Cu–Cl bond of the weaker π-hole interaction **B**, despite the presence of a weak and 'bent' π-hole motif, we do not observe any elongation and the bond length is close to average lengths reported in the Cambridge Structural Database.[44] Both X and Cl have the closest intermolecular contact with carbon atoms of carbonyl groups (C1 and C4), which are the most electron-depleted ones in the tetrachloroquinone molecule.

The topology of theoretical electron density[53] computed for **1** revealed the notably different nature of I···quinone and Cl···quinone interactions **A** and **B** (Table 2 and Fig. 2a). For the former contact, a single bond critical point (BCP) is found between I1 and the carbonyl C1 atom of the quinone. Its energy density ratio $\lvert V(\mathbf{r}_{CP})\rvert/G(\mathbf{r}_{CP})$ is <1,[56] indicating a purely electrostatic character. On the other hand, Cl···quinone interaction **B** involves four BCPs with lower electron densities, three of them between the terpyridyl moiety and the quinone (Table 2 and Fig. 2d). This points to a non-localized, dispersive interaction akin to the π-stacking of aromatic rings[58,59] and is

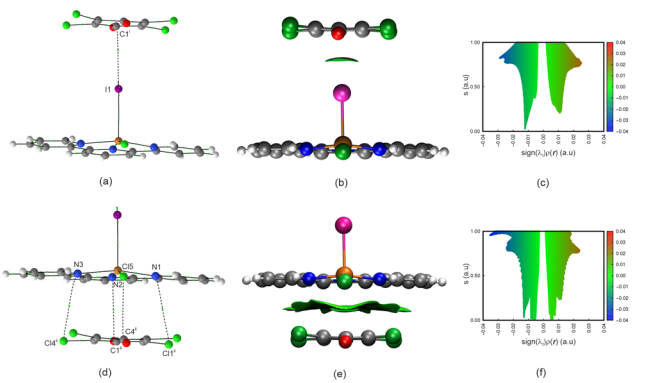

Fig. 2 Molecular graphs with intermolecular bond paths shown as dashed lines (a and d), reduced density gradient isosurfaces (b and e) and fingerprint plots of the reduced density gradient (RDG) against electron density multiplied by the sign of the second eigenvalue λ_2 of the Hessian matrix (c and f), in the region of π-hole interactions. Colour scheme of the fingerprint plots and RDG isosurfaces: blue – attractive interactions, green – van der Waals, red – repulsive interactions. Gradient surfaces are plotted at the 0.1 au level. Symmetry codes: (i) −1/2 + *x*, 3/2 − *y*, 1/2 + *z*, (ii) 1/2 + *x*, 3/2 − *y*, 1/2 + *z*.

also well reflected in the shape of the gradient of electron density (RDG) isosurfaces (compare Fig. 2b and e).[60,61] The domain attributed to chlorine π-hole interaction is broad with a multi-shape characteristic without distinctive directionality, whereas RDG assigned to iodine π-hole **A** is small and well-defined, indicating both directional and attractive characteristics. Interestingly, in both cases, one can identify a similar bluish spike on the far left side of the fingerprint plots (see Fig. 2c and f), which can be associated with the π-hole; however only in the case of chlorine π-hole additional van der Waals interactions can be identified (see green spikes close to zero). Furthermore, when calculating the integral of electron density with the formula $I_n = \int_{\Omega_a} \rho^n(\mathbf{r})\mathrm{d}\mathbf{r}$, one can also extract information on the volume ($n = 0$) and charge ($n = 1$) enclosed by the non-covalent interaction region (NCI). The volume of the RDG domain attributed to the iodine π-hole contact is 43.21 au, whereas the one assigned to chlorine π-hole is *ca.* 3.5 times bigger being 179.04 au. Similar dependence is observed for charges confined by the NCI region, giving values of 0.42 and 1.293, respectively.

Analogous information is provided when calculating interaction energies of the two π-hole motifs. They are calculated using the formula:

$$\Delta E_{\mathrm{int}}^{\mathrm{AB}} = E_{\mathrm{AB}} - (E_{\mathrm{A}} + E_{\mathrm{B}}) + \delta_{\mathrm{AB}}^{\mathrm{BSSE}}$$

where E_{AB} is the energy of a dimer, E_{A} and E_{B} are energies of the monomers (here E_{A} refers to quinone molecules and E_{B} to the [Cu(terpy)I_2] moiety) and $\delta_{\mathrm{AB}}^{\mathrm{BSSE}}$ is a correction removing artificial energy lowering caused by the basis set superposition error (BSSE).[62,63] The interaction energy for I···quinone contact **A** is −20.79 kcal mol^{-1}, approximately double that in the analogous contact with an uncoordinated iodide[41] and may be considered a very strong π-hole interaction attributed to a higher degree of polarisation along the bond path.[64,65] This aligns well with the elongation of the Cu–I bond and the distribution of electrostatic potential in the area of the π-hole interaction as shown in Fig. 3. The electrostatic potential map (Fig. 3) suggests that the iodine substituent is involved in the π-hole interaction which could also be classified as anion–π interaction; however, with the difference that the anion is in fact bound to the metal ion. The region of negative electrostatic potential points towards the conjugated system, along the Cu–I bond, whereas in the region perpendicular to the Cu–I bond, one observes positive electrostatic potential. The interaction energy for the Cl···quinone contact **B** is found to be −25.74 kcal mol^{-1}; however, this value includes not only the chlorine π-hole interaction, but also the other van der Waals interactions identified *via* QTAIM and NCI analysis (see Fig. 2d–f and Table 2). Thus, one can expect that the true energy of the π-hole interaction **B** would be half or less of the reported value, which would correspond to a typical weak non-covalent interaction.

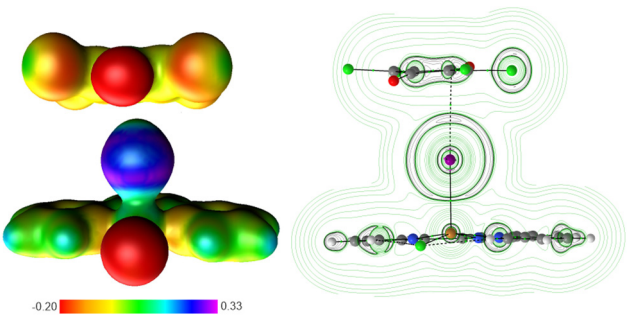

Fig. 3 (a) Electrostatic potential mapped on the electron density isosurface of 0.025 e Bohr^{-3} and (b) contour map of Laplacian of electron density (right) representing iodine π-hole interactions. Green and black lines correspond to positive and negative regions $\nabla^2\rho(\mathbf{r})$, respectively.

The π-hole interaction involves charge transfer, mostly influenced by iodide-to-quinone contribution, which is supported by the observed colour changes, resembling those seen in co-crystals with an uncoordinated iodide:[37,39,41] while the neutral perhaloquinones and complexes [Cu(terpy)X_2] appear yellow, the iodide-containing co-crystals **1** and **2** are black and opaque. In contrast, co-crystals **3** and **4**, which incorporate bromide instead of iodide, are pale green and transparent. These observations suggest that a significant degree of charge transfer is achievable only with the less electronegative and highly polarizable iodide, whereas charge transfer between bromide and quinone appears negligible.

Crystal packing of compounds **1–4** is dominated by infinite chains of π-hole interactions in an alternating fashion ···Q···X–Cu–Cl···Q···X–Cu–Cl···Q··· (*i.e.* alternating contacts ···**A**···**B**···**A**···**B**···) extending in [100] (Fig. 1b). The crystals grow as rods elongated in this direction; therefore, it was possible to apply electric contacts to opposite ends of single crystals and measure electric conductivity. The crystals behave as weak semiconductors with DC conductivities at 80° C being 10^{-11} to 10^{-9} S cm^{-1} (Fig. 4a, Table 3). The band structure (Fig. 4b) calculated for compound **1** confirms the experimental findings, with a band gap magnitude of 1.66 eV being typical for metal–organic semiconducting crystalline materials. This behaviour is particularly evident when examining the density of states of the elements and atomic orbitals of the interacting species. The dominant contribution to the top of the valence band is attributed to the iodine atom, specifically its p orbitals (see Fig. 4c and d). Additionally, a minor contribution near the top of the valence band is assigned to d–d transitions of the copper ion. Such insights strongly suggest that the charge transfer mechanism is primarily governed by π-hole interactions, with a slight cooperative contribution from the d–d transitions of the copper ion. Since there are no other intermolecular interactions parallel to [100], the observed conductivity is ascribed predominantly to these π-hole interactions. The intermolecular charge transport (*i.e.* conductivity) along the direction [100] involves two intermolecular contacts with different geometries and thus different energy barriers: X···quinone through contact **A** and quinone···Cl through contact **B**. The frontier orbital drawing (Fig. 5) shows that a lobe of the HOMO orbital extends from Cu through X, being here predominantly localized, into the π-system of the quinone and is then easily transferred to a LUMO orbital of the

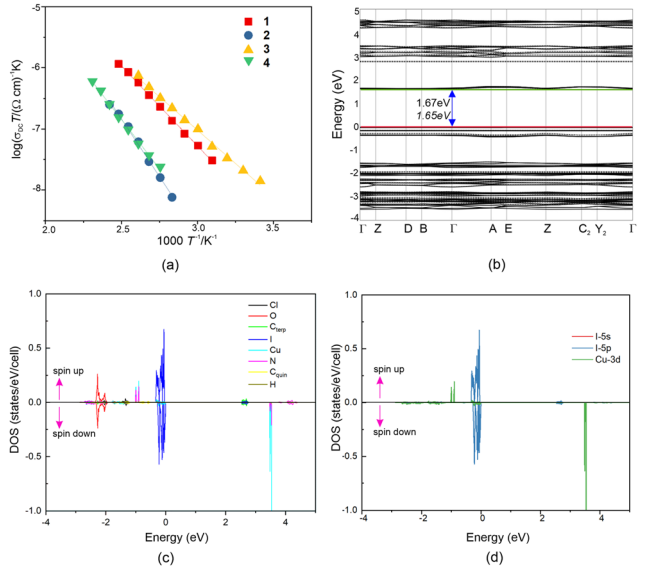

Fig. 4 (a) Arrhenius plot of temperature dependence of DC conductivity [$\log(\sigma_{DC})$ *vs.* 1000/*T*] for the four studied compounds. (b) Electronic band structure of compound **1** obtained from spin-polarized unrestricted periodic-DFT calculations. Solid and dashed lines refer to α and β spin polarization (energy gap values given in italics), respectively. (c) Atom-projected density of states (DOS) of compound **1**. The positive and negative values represent the DOS of up and down spins, respectively. Scaling factor of 10^{-2} used. (d) Density of states projected on the s, p and d atomic orbitals of iodine and copper, respectively. The energy axis in b–d is shifted upwards by 5.43 eV, so as to place the Fermi level at the origin (E = 0).

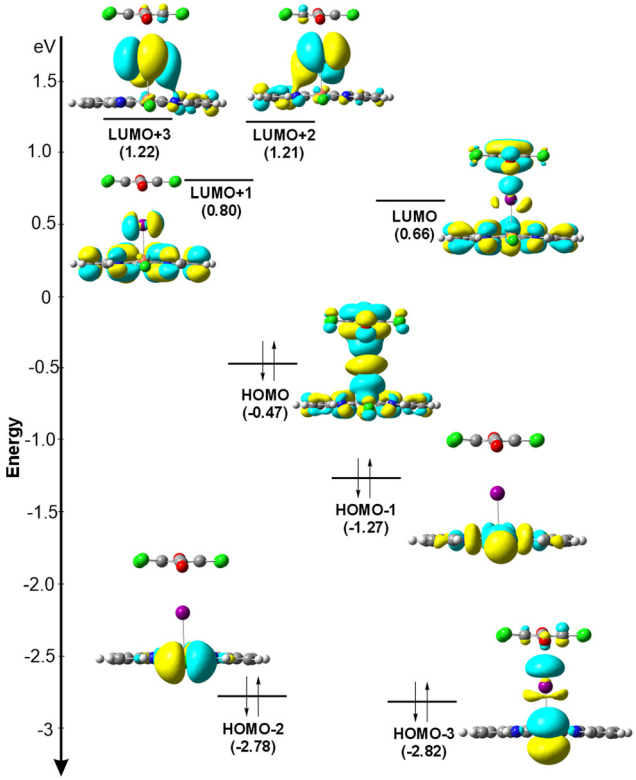

Fig. 5 Selected frontier molecular orbitals in the region of iodine π-hole interaction (contact **A**), calculated for an isolated dimer of tetrachloroquinone and the [Cu(terpy)ClI] moiety, assuming gas phase conditions. Surfaces are drawn at an isovalue of 0.02 au.

Table 3 DC conductivity (σ_{DC}) at 80 °C and activation energy (E_{DC}) of the studied compounds

Compound	$\log(\sigma_{DC}/(\Omega\ cm)^{-1})^a$	E_a/eV
1	−9.41	0.52
2	−10.67	0.75
3	−9.20	0.43
4	−10.29	0.64

[a] At 20 °C.

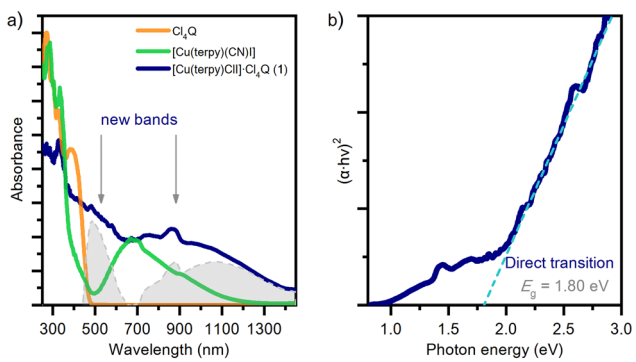

Fig. 6 Solid-state UV-vis diffuse reflectance spectroscopy: (a) absorption spectra of [Cu(terpy)ClI]·Cl_4Q (**1**), [Cu(terpy)(CN)I] and tetrachloroquinone Cl_4Q (grey area indicates additional absorption in the spectra of **1** compared to [Cu(terpy)(CN)I] and Cl_4Q); (b) Tauc's plot of [Cu(terpy)ClI]·Cl_4Q (**1**) corresponding to direct transitions.

quinone. This indicates that charge transfer through contact **A** should be facile, and the energy barrier is rather low. On the other hand, the weaker interaction, and therefore the step which limits conductivity is through contact **B**. This explains the similar conductivities of all four compounds discussed here (Table 3), and suggests that electron transport through the stronger interaction (contact **A**) should be much more favourable with a much lower energy barrier.

The experimental optical diffuse reflectance spectra of complexes **1–4**, the starting reagent tetrachloroquinone Cl_4Q and the complex [Cu(terpy)(CN)I][66] were measured in the range of 200–1500 nm (Fig. 6 and Fig. S19†). The tetrachloroquinone begins to absorb light at the edge of the visible spectrum, with the absorption band with the lowest energy at 390 nm. This peak and the peaks detected in the UV part of the spectrum at 296 and 325 nm are characteristic of intraligand transitions in the quinone system. The complex [Cu(terpy)(CN)I] with a similar copper(II) coordination environment[66] as in compounds **1** and **2** exhibits a visible absorption band at 670 nm: this band corresponds to a d–d transition for copper(II) in a five-coordinate square-pyramidal environment.[67] In addition

to the peaks appearing in the starting reagent Cl_4Q and in the complex with a similar copper(II) geometry [Cu(terpy)(CN)I], compounds **1** and **2** show two new absorption maxima located at ~483 nm and ~1072 nm. These bands are most likely associated with the formation of charge transfer adducts, more specifically with the interaction between [Cu(terpy)ClI] and tetrachloroquinone, likely corresponding to two types of π-hole contacts between a metal-bonded halide and a quinoid ring in compound **1** (**A** and **B** in Fig. 1b). The shorter contact, labelled **A** (Fig. 1b), could be responsible for the lower energy charge transfer transitions appearing as a broad band centred at 1072 nm, while the band at 483 nm could originate from a higher energy charge transfer transition labelled as contact **B** (Fig. 1b). The absence of these bands in the spectra of compounds **3** and **4** (Fig. S19†), where no charge transfer is expected according to the structural analysis, is also a confirmation that the new absorption bands in **1** and **2** are due to strong π-hole contacts. TD-DFT calculations performed on the contact **A** dimer of compound **1** further corroborate these experimental findings (see ESI, Fig. S12–S14†). The calculations predict a HOMO–LUMO transition at 1097 nm, in excellent agreement with the experimentally observed absorption band at 1072 nm. Additionally, the TD-DFT results provide detailed insights into the electronic transitions, confirming that the HOMO is delocalized across the [Cu(terpy)ClI] complex and the LUMO is localized on the π-system of the quinone. This supports the assignment of the absorption bands to charge transfer processes involving these strong π-hole contacts (see Fig. S12†). The inclusion of oscillator strength values and calculated excitation energies strengthens the claim that these transitions arise from cooperative charge transfer mechanisms rather than isolated intraligand or d–d transitions, providing further validation for the structural and spectroscopic analyses.

Tauc's plots from diffuse reflectance measurements were calculated to estimate the band gap energy of compound **1**. According to Tauc's plot, compound **1** has a direct band gap at a photon energy of 1.80 eV. The results shown in Fig. 6b agree well with the values calculated from DFT, which indicate a band gap of 1.66 eV.

Conclusions

We have described a series of four novel isostructural co-crystals [Cu(terpy)ClX]·X'_4Q with strong π-hole interactions between a metal-bound halide and a quinoid ring. The combined data strongly support a charge transfer pathway involving the entire [Cu(terpy)ClI] complex, with iodine playing a pivotal role in facilitating the interaction through π-hole interaction, which is reflected in the black colour of the crystals. This interpretation is supported by the observed optical absorption spectra and band structure calculations, which highlight the interplay of these transitions in shaping the electronic properties.

Although conductivities of compounds **1–4** are rather low, they nevertheless show that conductivity through the π-hole interaction can be achieved and may be enhanced by crystal engineering. An infinite chain of ···iodide···quinone···iodide··· moieties may increase conductivity by several orders of magnitude. We anticipate that by a smart choice of electron donors and electron acceptors, one can substantially enhance the effect and engineer more efficient conductive materials.

Also, co-crystals of this type are easily prepared and are stable – after more than a year out of the matrix, in air and at room temperature, the crystals did not show any sign of decomposition. Therefore, π-hole interactions seem to have much potential in crystal engineering and materials chemistry.

Another interesting observation is that we obtained the compounds [Cu(terpy)ClX] only as co-crystals with quinones. All attempts for the preparation of pure compounds [Cu(terpy)ClX] were unsuccessful. Instead, mixtures of [Cu(terpy)Cl_2] and [Cu(terpy)X_2] were obtained, and the presence of a novel phase, which may be [Cu(terpy)ClI], was not detected. Since we were able to obtain [Cu(terpy)ClX] only as a co-crystal with the quinones, we conclude that [Cu(terpy)ClX] is thermodynamically less stable than [Cu(terpy)Cl_2] and [Cu(terpy)X_2] and forms only in the presence of quinones, as it is stabilised by π-hole interactions.

Experimental

Single crystals of the compounds **1–4** were prepared by applying a layering technique using analogue syntheses. A mixture of methanol solution (4 mL) of $CuCl_2{\cdot}2H_2O$ (0.017 g; 0.100 mmol) and 2,2′:6′,2″-terpyridine (0.023 g; 0.100 mmol) was layered with a mixture of acetonitrile solutions (6 mL) of tetrachloro- or tetrabromoquinone, ($C_6O_2Cl_4$ or $C_6O_2Br_4$, 0.040 mmol) and KI (0.020 g; 0.012 mmol) After a few days, black crystals of **1** and **2** or green crystals of **3** and **4** were formed, respectively, isolated, washed with water and dried in air.

Single crystal measurements were performed on a dual source (Mo/Cu) Rigaku Oxford Diffraction Synergy S diffractometer equipped with an Oxford Cryosystems Series 800 cryostat. The program package CrysAlis PRO[68] was used for data reduction and analytical absorption correction. The structures were solved using SHELXS97[69] and refined with SHELXL-2017.[70] The models were refined using the full-matrix least squares refinement; all non-hydrogen atoms were refined anisotropically. Hydrogen atoms were located in a difference Fourier map and refined as riding entities. In **3** a substitutional disorder is present with the Cu-bound atom Cl5 being partially substituted with a bromine, labelled as Br2. The refined occupancies are 0.65 and 0.35, respectively.

Periodic DFT computations for **1** were performed by the CRYSTAL23 software.[71] Calculations were performed as spin-polarized unrestricted DFT using PBE0 hybrid functional with Grimme D3 dispersion correction,[72] at the pob-DZVP level of theory. For topological analysis of electron density, program TOPOND23[73] fully integrated with CRYSTAL23 was used. To support the discussion on the nature of chemical bonding in

the studied system, single-point gas-phase calculations on interacting dimers including halogen-quinone and π-hole contacts were performed at the DFT/PBE0/def2-TZVP level[74,75] using the GAUSSIAN 16.C.01 program package.[76] Gas-phase wavefunctions were used to generate the electrostatic potential of interacting molecules and analyse molecular orbitals of the studied dimers. The same wavefunctions were further used to analyse electron density distribution with the AIMAll package[77] and to perform quantitative NCI-analysis (non-covalent interactions analysis) by generating reduced density gradients (RDGs) and calculating electron density derived properties within the RDG regions. All NCI related calculations were performed using NCIPLOT4 software.[78]

The electrical properties were studied by solid-state impedance spectroscopy (ss-IS) on single crystals along the direction of the π-hole chains (the long axis of rod-like crystals) using an impedance analyzer (Novocontrol Alpha-AN Dielectric Spectrometer, Novocontrol Technologies, Montabaur, Germany), at a voltage of 20 mV under a nitrogen atmosphere over the temperature range from −30 to 80 (±0.5) °C and frequencies from 0.1 Hz to 1 MHz. The impedance spectra were analysed by equivalent circuit modelling using the complex nonlinear least-squares fitting procedure (ZView software). The complex impedance plane in both crystal orientations displays an arc which can be modelled by an equivalent circuit consisting of a resistor and a capacitor in parallel.

Solid-state UV-vis diffuse reflectance spectroscopy was performed on a Shimadzu UV-Vis-NIR spectrometer (model UV-3600) equipped with an integrating sphere. Barium sulphate was used as a reference. The diffuse reflectance spectra were transformed using the Kubelka–Munk function and the optical bandgaps were estimated from Tauc's plots.

Author contributions

L. M. – synthesis, IR spectroscopy, analysis of crystal structures, and writing – review & editing. A. K. – conceptualization, quantum chemical computations, and writing – original draft, review & editing. L. P. – impedance spectroscopy measurements. M. J. – conceptualization, synthesis, and writing – review & editing. L. A. D. – TG/DSC and UV/vis spectroscopy. K. M. – conceptualization, crystallography, analysis of crystal structures, and writing – original draft, review & editing.

Data availability

The data that support the structures and plots within this paper and other findings of this study are available from the corresponding authors upon reasonable request.

Conflicts of interest

There are no conflicts to declare.

Acknowledgements

This work was financed by the Croatian Science Foundation, grant no. 2019-04-4674, IP-2024-05-8711 and IP-2019-04-5742. We gratefully acknowledge Polish high-performance computing infrastructure PLGrid (HPC Centers: ACK Cyfronet AGH) for providing computer facilities and support under computational grant no. PLG/2022/015866.

References

1 E. Coronado and P. Day, *Chem. Rev.*, 2004, **104**, 5419–5448.
2 E. Coronado, C. Gimenez-Saenz and C. J. Gomez-Garcia, *Coord. Chem. Rev.*, 2005, **249**, 1776–1796.
3 I. Ratera and J. Veciana, *Chem. Soc. Rev.*, 2012, **41**, 303–349.
4 S. Sanvito, *Chem. Soc. Rev.*, 2011, **40**, 3336–3366.
5 E. Coronado, J. R. Galan-Mascaros, C. J. Gomez-Garcia and V. Laukhin, *Nature*, 2000, **408**, 447–449.
6 M. Atzori, F. Pop, P. Auban-Senzier, R. Clerac, E. Canadell, M. L. Mercuri and N. Avarvari, *Inorg. Chem.*, 2015, **54**, 3643–3653.
7 C. F. Leong, P. M. Usov and D. M. D'Alessandro, *MRS Bull.*, 2016, **41**, 858–864.
8 M. L. Mercuri, F. Congiu, G. Concas and S. A. Sahadevan, *Magnetochemistry*, 2017, **3**, 17.
9 S. A. Sahadevan, A. Abherve, N. Monni, C. Saenz de Pipaon, J. R. Galan-Mascaros, J. C. Waerenborgh, B. J. C. Vieira, P. Auban-Senzier, S. Pillet, E. Bendeif, P. Alemany, E. Canadell, M. L. Mercuri and N. Avarvari, *J. Am. Chem. Soc.*, 2018, **140**, 12611–12621.
10 Ö. Üngör and M. Shatruk, *Polyhedron*, 2019, **177**, 114254.
11 S. A. Sahadevan, A. Abherve, N. Monni, P. Auban-Senzier, J. Cano, F. Lloret, M. Julve, H. Cui, R. Kato, E. Canadell, M. L. Mercuri and N. Avarvari, *Inorg. Chem.*, 2019, **58**, 15359–15370.
12 S. A. Sahadevan, A. Abherve, N. Monni, P. Auban-Senzier, H. Cui, R. Kato, M. L. Mercuri and N. Avarvari, *Cryst. Growth Des.*, 2020, **20**, 6777–6786.
13 A. Abherve, N. Mroweh, T. Cauchy, F. Pop, H. Cui, R. Kato, N. Vanthuyne, P. Alemany, E. Canadell and N. Avarvari, *J. Mater. Chem. C*, 2021, **9**, 4119–4140.
14 P. A. Benavides, M. A. Gordillo, E. Thibodeaux, A. Yadav, E. Johnson, R. Sachdeva and S. Saha, *ACS Appl. Mater. Interfaces*, 2023, **16**, 1234–1242.
15 M. Shiotsuka, Y. Okaue, N. Matsumoto, H. Okawa and T. Isobe, *J. Chem. Soc., Dalton Trans.*, 1994, 2065–2070.
16 K. Molčanov, M. Jurić and B. Kojić-Prodić, *Dalton Trans.*, 2013, **42**, 15756–15765.
17 M. Jurić, K. Molčanov, D. Žilić and B. Kojić-Prodić, *RSC Adv.*, 2016, **6**, 62785–62769.
18 B. L. Schottel, H. L. Chifotides, M. Shatruk, A. Chouai, L. M. Perez, J. Bacsa and K. R. Dunbar, *J. Am. Chem. Soc.*, 2006, **128**, 5895–5912.
19 S. Demeshko, S. Dechert and F. Meyer, *J. Am. Chem. Soc.*, 2004, **126**, 4508–4509.

20 S. V. Lindeman, J. Hecht and J. K. Kochi, *J. Am. Chem. Soc.*, 2003, **125**, 11597–11606.
21 Y. S. Rosokha, S. V. Lindeman, S. V. Rosokha and J. K. Kochi, *Angew. Chem., Int. Ed.*, 2004, **43**, 4650–4652.
22 B. L. Schottel, H. T. Chifotides and K. R. Dunbar, *Chem. Soc. Rev.*, 2008, **37**, 68–83.
23 T. J. Mooibroek, P. Gamez and J. Reedijk, *CrystEngComm*, 2008, **10**, 1501–1515.
24 A. Frontera, P. Gamez, M. Mascal, T. J. Mooibroek and J. Reedijk, *Angew. Chem., Int. Ed.*, 2011, **50**, 9564–9583.
25 D.-X. Wang and M.-X. Wang, *J. Am. Chem. Soc.*, 2013, **135**, 892–897.
26 S. K. Sing and A. Das, *Phys. Chem. Chem. Phys.*, 2015, **17**, 9596–9612.
27 S. Kozuch, *Phys. Chem. Chem. Phys.*, 2016, **18**, 30366–30369.
28 R. W. Newberry and R. T. Raines, *Acc. Chem. Res.*, 2017, **50**, 1838–1846.
29 O. Grounds, M. Zeller and S. V. Rosokha, *New J. Chem.*, 2018, **42**, 10572–10583.
30 V. Angarov and S. Kozuch, *New J. Chem.*, 2018, **42**, 1413–1422.
31 X. Lucas, A. Bauza, A. Frontera and D. A. Quiñonero, *Chem. Sci.*, 2016, **7**, 1038–1050.
32 A. Bauza, T. J. Mooibroek and A. Frontera, *CrystEngComm*, 2016, **18**, 10–23.
33 M. Savastano, C. Bazzicalupi, C. García, C. Gellini, M. D. Lopez de la Torre, P. Mariani, F. Pinchierri, A. Bianchi and M. Melguizo, *Dalton Trans.*, 2017, **46**, 4518–4529.
34 S. Kumar Seth, A. Bauzá, G. Mahmoudi, V. Stilinović, E. López-Torres, G. Zaragoza, A. D. Keramidas and A. Frontera, *CrystEngComm*, 2018, **20**, 5033–5044.
35 C. Jia, H. Miao and B. P. Hay, *Cryst. Growth Des.*, 2019, **19**, 6806–6821.
36 S. Kumar Seth, A. Bauzá and A. Frontera, Quantitative Analysis of Weak Non-covalent σ-Hole and π-Hole Interactions, in *Understanding Intermolecular Interactions in the Solid State: Approaches and Techniques*, ed. D. Chopra, Royal Society of Chemistry, London, 2019.
37 K. Molčanov, G. Mali, J. Grdadolnik, J. Stare, V. Stilinović and B. Kojić-Prodić, *Cryst. Growth Des.*, 2018, **18**, 5182–5193.
38 (*a*) S. Kepler, M. Zeller and S. V. Rosokha, *J. Am. Chem. Soc.*, 2019, **141**, 9338–9348; (*b*) J. Wilson, T. Maxson, I. Wright, M. Zeller and S. V. Rosokha, *Dalton Trans.*, 2020, **49**, 8734–8743.
39 V. Milašinović and K. Molčanov, *CrystEngComm*, 2021, **23**, 8209–8214.
40 A. Shkurenko, *IUCrJ*, 2023, **10**, 145–146.
41 V. Milašinović, V. Vuković, A. Krawczuk, K. Molčanov, C. Hennig and M. Bodensteiner, *IUCrJ*, 2023, **10**, 156–163.
42 H. Zeng, P. Liu, G. Feng and F. Huang, *J. Am. Chem. Soc.*, 2019, **141**, 16501–16511.
43 B. Han, J. Lu and J. K. Kochi, *Cryst. Growth Des.*, 2008, **8**, 1327–1334.
44 C. R. Groom, I. J. Bruno, M. P. Lightfoot and S. C. Ward, *Acta Crystallogr., Sect. B: Struct. Sci., Cryst. Eng. Mater.*, 2016, **72**, 171–179.
45 C. J. Kingsbury, B. F. Abrahams and R. Robson, Private communication, 2017, CCDC entry no. 1568040, refcode TAZSIZ.
46 M. Strianese, S. Milione, V. Bertolasi, C. Pellechia and A. Grassi, *Inorg. Chem.*, 2011, **50**, 900–910.
47 C. Uechi, H. Yamaguchi, I. Ueda and K. Yasukouchi, *Bull. Chem. Soc. Jpn.*, 1980, **53**, 3483–3487.
48 A. Kobayashi, M. Dosen, M. Chang, K. Nakajima, S. Noro and M. Kato, *J. Am. Chem. Soc.*, 2010, **132**, 15286–15298.
49 S. Stang, A. Lebkücher, P. Walter, E. Kaifer and H.-J. Himmel, *Eur. J. Inorg. Chem.*, 2012, **51**, 4833–4845.
50 A. Kutoglu, R. Allmann, J.-V. Folgado, M. Atanasov and D. Reinen, *Z. Naturforsch., B: J. Chem. Sci.*, 1991, **46**, 1193–1199.
51 M. I. Arriortua, J. L. Mesa, T. Rojo, T. Debaerdemaeker, D. Beltran-Porter, H. Stratemeier and D. Reinen, *Inorg. Chem.*, 1988, **27**, 2976–2981.
52 G. P. Moss, *Pure Appl. Chem.*, 1996, **68**, 2193–2222.
53 R. F. W. Bader, *Atoms in Molecules: A Quantum Theory*, Oxford University Press, Oxford, 1990.
54 R. F. W. Bader, *J. Phys. Chem.*, 1988, **102**, 7314–7323.
55 D. Cremer and E. Kraka, *Angew. Chem., Int. Ed. Engl.*, 1984, **23**, 627–628.
56 Y. Abramov, A. Volkov, G. Wu and P. Coppens, *Acta Crystallogr., Sect. A: Found. Crystallogr.*, 2000, **56**, 585–591.
57 L. J. Farrugia, C. Evans, D. Lentz and M. Roemer, *J. Am. Chem. Soc.*, 2009, **131**, 1251–1268.
58 K. Molčanov and B. Kojić-Prodić, *IUCrJ*, 2019, **6**, 155–166.
59 K. Molčanov, V. Milašinović and B. Kojić-Prodić, *Cryst. Growth Des.*, 2019, **19**, 5967–5980.
60 J. Contreras-García, E. R. Johnson, S. Keinan, R. Chaudret, J.-P. Piquemal, D. N. Beratan and W. Yang, *J. Chem. Theory Comput.*, 2011, **7**, 625–632.
61 E. R. Johnson, S. Keinan, P. Mori-Sánchez, J. Contreras-García, A. J. Cohen and W. Yang, *J. Am. Chem. Soc.*, 2010, **132**, 6498–6506.
62 N. R. Kestner, *J. Chem. Phys.*, 1968, **48**, 252–257.
63 B. Liu and A. D. McLean, *J. Chem. Phys.*, 1973, **59**, 4557–4558.
64 P. Poltizer, J. S. Murray and T. Clark, *J. Phys. Chem. A*, 2019, **123**, 10123–10130.
65 P. Politzer, J. S. Murray and T. Clark, *Phys. Chem. Chem. Phys.*, 2021, **23**, 16458–16468.
66 L. Molčanov, K. Molčanov and M. Jurić, to be published.
67 Y. Mikata, M. Akedo, E. Hamamoto, S. Yoshida, S. Shoji, T. Storr, Y. Funahashi and T. Matsuo, *Dalton Trans.*, 2024, **53**, 16716–16732.
68 O.D. Rigaku, *P.R.O. CrysAlis, version: 1.171.39.46*, Rigaku Oxford Diffraction Ltd, Yarnton, England, 2018.
69 G. M. Sheldrick, *Acta Crystallogr., Sect. A: Found. Adv.*, 2015, **71**, 3–8.
70 G. M. Sheldrick, *Acta Crystallogr., Sect. C:Struct. Chem.*, 2015, **71**, 3–8.

71 (*a*) A. Erba, J. K. Desmarais, S. Casassa, B. Civalleri, L. Donà, I. J. Bush, B. Searle, L. Maschio, L.-E. Daga, A. Cossard, C. Ribaldone, E. Ascrizzi, N. L. Marana, J.-P. Flament and B. Kirtman, *J. Chem. Theory Comput.*, 2023, **19**, 6891–6932; (*b*) R. Dovesi, V. R. Saunders, C. Roetti, R. Orlando, C. M. Zicovich-Wilson, F. Pascale, B. Civalleri, K. Doll, N. M. Harrison, I. J. Bush, Ph. D'Arco, M. Llunell, M. Causà, Y. Noeul, L. Maschio, A. Erba, M. Rerat, S. Casassa, B. G. Searle and J. K. Desmarais, *CRYSTAL23 User's Manual*, University of Torino, Torino, 2023.

72 S. Grimme, J. Antony, S. Ehrlich and H. A. Krieg, *J. Chem. Phys.*, 2010, **132**, 154104.

73 C. Gatti, S. Casassa, J. K. Desmarais, A. Cossard and A. Erba, *TOPOND23 User's Manual*, CNR-ISTM, Milan, Italy, 2022.

74 C. Adamo and V. J. Barone, *J. Chem. Phys.*, 1999, **110**, 6158–6170.

75 F. Weigend and R. Ahlrichs, *Phys. Chem. Chem. Phys.*, 2005, **7**, 3297–3305.

76 M. J. Frisch, G. W. Trucks, H. B. Schlegel, G. E. Scuseria, M. A. Robb, J. R. Cheeseman, G. Scalmani, V. Barone, G. A. Petersson, H. Nakatsuji, X. Li, M. Caricato, A. V. Marenich, J. Bloino, B. G. Janesko, R. Gomperts, B. Mennucci, H. P. Hratchian, J. V. Ortiz, A. F. Izmaylov, J. L. Sonnenberg, D. Williams-Young, F. Ding, F. Lipparini, F. Egidi, J. Goings, B. Peng, A. Petrone, T. Henderson, D. Ranasinghe, V. G. Zakrzewski, J. Gao, N. Rega, G. Zheng, W. Liang, M. Hada, M. Ehara, K. Toyota, R. Fukuda, J. Hasegawa, M. Ishida, T. Nakajima, Y. Honda, O. Kitao, H. Nakai, T. Vreven, K. Throssell, J. A. Montgomery Jr., J. E. Peralta, F. Ogliaro, M. J. Bearpark, J. J. Heyd, E. N. Brothers, K. N. Kudin, V. N. Staroverov, T. A. Keith, R. Kobayashi, J. Normand, K. Raghavachari, A. P. Rendell, J. C. Burant, S. S. Iyengar, J. Tomasi, M. Cossi, J. M. Millam, M. Klene, C. Adamo, R. Cammi, J. W. Ochterski, R. L. Martin, K. Morokuma, O. Farkas, J. B. Foresman and D. Fox, *D. J. Gaussian 16, Revision C.01*, Gaussian, Inc., Wallingford CT, 2016.

77 T. A. Keith, *AIMAll (Version 19.10.12)*, TK Gristmill Software, Overland Park, KS, 2019, **https://aim.tkgristmill.com** (accessed: August, 2023).

78 R. A. Boto, F. Peccati, R. Laplaza, C. Quan, A. Carbone, J.-P. Piquemal, Y. Maday and J. Contreras-Garcia, *J. Chem. Theory Comput.*, 2020, **16**, 4150–4158.